Available online at www.sciencedirect.com
ScienceDirect
Journal of Power Sources 179 (2008) 412–416
JOURNAL OF POWER SOURCES
www.elsevier.com/locate/jpowsour

Short communication

In-situ study of the cracking of metal hydride electrodes by acoustic emission technique

S. Didier-Laurent [a,b], H. Idrissi [a], L. Roué [b,*]

[a] *MATEIS - RI2S, INSA - Lyon, Bât L. de Vinci, 21 Avenue Jean Capelle, 69621 Villeurbanne Cedex, France*
[b] *INRS - Energie, Matériaux et Télécommunications, 1650 Boulevard Lionel Boulet, Varennes, Québec, Canada J3X 1S2*

Received 28 September 2007; received in revised form 6 December 2007; accepted 14 December 2007
Available online 28 December 2007

Abstract

Pulverisation phenomena occurring during the charge/discharge cycling of metal hydride materials were studied by acoustic emission coupled to electrochemical measurements. Two kinds of materials were studied: a commercial $LaNi_5$-based alloy and a ball-milled MgNi alloy. In both alloys, two populations of acoustic signals were detected during charging steps: P1, showing peak frequencies between 230 and 260 kHz, high energy and low rise time, and P2 with peak frequencies between 150 and 180 kHz, lower energy and longer rise time. Population P2 is related to the hydrogen evolution reaction whereas P1 is associated with pulverisation phenomena. No acoustic activity was detected during discharge. We also investigated pulverisation phenomena through cycles by monitoring the P1 population. It appears that pulverisation occurs mainly during the five first cycles for $LaNi_5$ with a maximum at the second cycle, while pulverisation takes place all along the cycling for MgNi, but at a decreasing rate. By comparing the P1 activities, it appears that the pulverization phenomenon is less intensive on the MgNi electrode than on the $LaNi_5$-based electrode.

Keywords: Acoustic emission; Particle cracking; Metal hydride electrodes; Ni–MH batteries

1. Introduction

In Ni–MH batteries, the cracking of the metal hydride (MH) particles in the negative electrode has a strong influence on the battery performance. This phenomenon, which occurs mainly during the first charge/discharge cycles, is attributed to the MH lattice expansion through the hydrogen absorption reaction. In the case of $LaNi_5$-based materials, the particle cracking activates the MH electrode by breaking the native oxide layer present at the surface of the particles and by increasing the effective surface area of the electrode [1]. On the other hand, the particle pulverization has a negative effect on the electrode cycle life by increasing the corrosion rate of the AB_5 alloy [2]. In the case of MgNi-based materials, it was demonstrated that the key to obtaining stable electrodes is to limit their pulverization upon cycling [3]. Thus, the evaluation of the MH particle cracking has a central importance in the search for high performance negative electrodes for Ni–MH batteries.

Particle pulverisation is usually evaluated using *ex-situ* methods such as scanning electron microscopy (SEM) or surface area measurements by the Brunauer–Emmet–Tellet (BET) method [1,2]. However, the first method is only qualitative and the latter method is not precise since the results can be strongly altered by the hydroxides produced during cycling and the additives used to form a conductive electrode. The particle pulverization was studied *in-situ* by measuring the evolution with cycling of the hydrogen diffusion coefficient to particle radius ratio (D/a^2) using the potential step technique [4,5]. However, this method presents some limitations due to the assumptions (e.g. particle sphericity) used for the data treatment [5]. Thus, more powerful methods for *in-situ* monitoring of the MH particle pulverization have to be developed.

Acoustic emission (AE) is a non-destructive technique (NDT), defined by the American Society for the Testing of Materials (ASTM) as "the class of phenomena whereby transient elastic waves are generated by the rapid release of energy from localized sources within the material" [6], such as crack initiation and propagation, but also gas evolution or thin film rupture. For few years, AE has been successfully applied to the study

* Corresponding author. Tel.: +1 450 929 8185; fax: +1 450 929 8102.
E-mail address: roue@emt.inrs.ca (L. Roué).

0378-7753/$ – see front matter © 2007 Elsevier B.V. All rights reserved.
doi:10.1016/j.jpowsour.2007.12.073

of various corrosion and electrochemical phenomena [7–9], but only few papers have dealt with the study of the pulverization of metal hydride electrodes [10–12].

In this paper, we propose to study the MH particle cracking by AE coupled to electrochemical measurements. In a first step, we will differentiate the various acoustic populations recorded during a charge/discharge cycle and link them to the electrochemical reactions that occur in the material. In a second step, we will follow the evolution of the acoustic activity upon cycling, in order to quantify the pulverisation phenomena. Two types of hydride materials will be studied: a commercial $LaNi_5$-based alloy and a MgNi alloy.

2. Experimental details

Two kinds of hydride materials were studied: a commercial $LaNi_5$-based alloy ($MmNi_{3.68}Co_{0.78}Mn_{0.36}Al_{0.28}$) from Japan Metals and Chemicals Co. and an amorphous MgNi alloy obtained by high energy ball milling (see Ref. [3] for more details).

The schema of the experimental set-up coupling AE and electrochemical measurements is shown in Fig. 1A. The electrochemical measurements were performed using a Voltalab PGZ 301 potentiostat and VoltaMaster 4 software, monitoring a three-electrode cell. The working electrode was composed of 0.2 g of active material mixed with 0.2 g of pure copper powder (75 mesh) and pressed on 2 g of pure copper powder under a pressure of 2.5 t cm^{-2}. The reference electrode and the counter electrode were respectively an Hg/HgO electrode (XR 400 from Radiometer Analytical) and a platinum wire (whose surface is large enough to avoid limitation on the work electrode). $LaNi_5$-based samples were charged at -100 mA g^{-1} for 3 h and discharged at 50 mA g^{-1} until -0.6 V versus Hg/HgO, while MgNi samples were charged at -200 mA g^{-1} for 3 h and discharged at 20 mA g^{-1} until -0.6 V versus Hg/HgO. All the experiments were carried out at room temperature in a 6 mol l^{-1} KOH solution.

The AE signals were recorded by a wide band sensor Vallen AE 144 A (frequency range 100–500 kHz) and transmitted via a preamplifier and a Vallen AMS3 acquisition card to a computer. For all the experiments, the gain G and the threshold S were respectively fixed at 49 dB and 27.4 dB, while the sampling rate was fixed at 4 MHz. The recorded acoustic signals were treated using Vallen AE software and the waveforms and power spectra were obtained with Matlab 7.1. Typical acoustic emission waveform is shown in Fig. 1B. From this diagram, characteristics of the recorded signal can be obtained, such as its amplitude, its duration, its rise time, or its energy. Rise time corresponds to the duration between the first threshold passing and the maximum signal amplitude. The energy of the acoustic signal is the integral of the squared amplitude over time of signal duration and is expressed in term of energy units (eu). One eu means 10^{-14} V^2s, corresponding to 10^{-18} J at a reference resistor of 10 kOhm.

3. Results and discussions

3.1. Correlation between acoustic activity and electrode potential

Fig. 2 represents the typical evolution of the acoustic activity versus time recorded during a charge/discharge cycle on $LaNi_5$-based electrodes. On the basis of the evolution of the acoustic activity, four stages can be distinguished. The stage (I) occurs in the first 40 min of charging, and is associated with a very low acoustic activity. From 40 to 120 min of charge, stage (II), the acoustic activity increases progressively. During this stage, the stabilization of the potential around -1.15 V versus Hg/HgO can be attributed to the formation of the hydride (β phase), leading to pulverization phenomena, hence increasing the acoustic activity. From 120 min up to the end of the charging period, stage (III), the acoustic activity increases strongly, while gas release can be observed on the sample. This is related to the hydro-

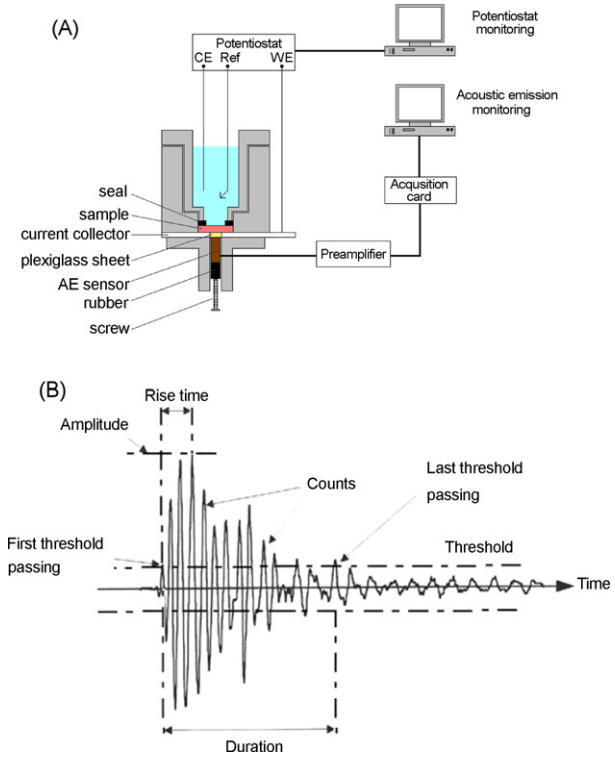

Fig. 1. (A) Schematic representation of the experimental set-up coupling AE and electrochemical measurements. (B) Main acoustic characteristics recorded on a typical waveform signal.

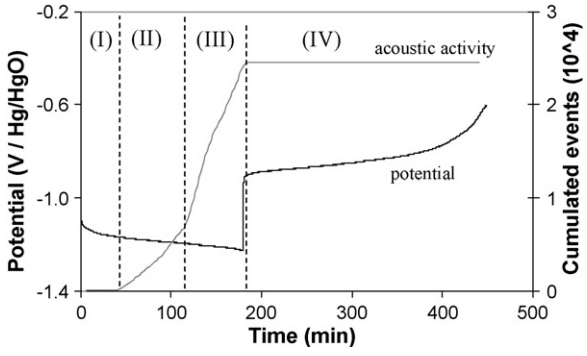

Fig. 2. Typical evolution of the AE activity vs. time recorded during a charge/discharge cycle on a $LaNi_5$-based electrode.

gen evolution reaction (HER), which is well known to be highly acoustic emissive. Finally, stage (IV) corresponds to the discharge step, during which no more acoustic activity is detected. This shows that the hydrogen desorption reaction is not emissive in the studied frequency range or is not energetic enough to be detected by AE techniques. Similar results were obtained on the MgNi electrode (not shown).

3.2. Analysis of the acoustic signals

Two kinds of acoustic signals were recorded whatever the materials. Fig. 3A shows the rise time versus energy of the recorded events during the first charge on the $LaNi_5$-based electrode. It clearly shows the presence of two populations, P1 and P2. While P1 exhibits a low rise time (<20 μs) and high energy (up to 40 eu), P2 is composed of low energy events (<10 eu) with high rise time (up to 200 μs). This interpretation is confirmed by the analysis of the recorded waveforms. Indeed, two main waveforms are observed throughout a charging step (Fig. 3B).

Table 1
Main characteristics of recorded AE populations

	Population P1	Population P2
Duration (μs)	20–30	50
Rise time (μs)	<20	up to 200
Energy (eu)	up to 40	<10
Frequency peak (kHz)	~250	150–200
Width of frequency peak (kHz)	~400	~200

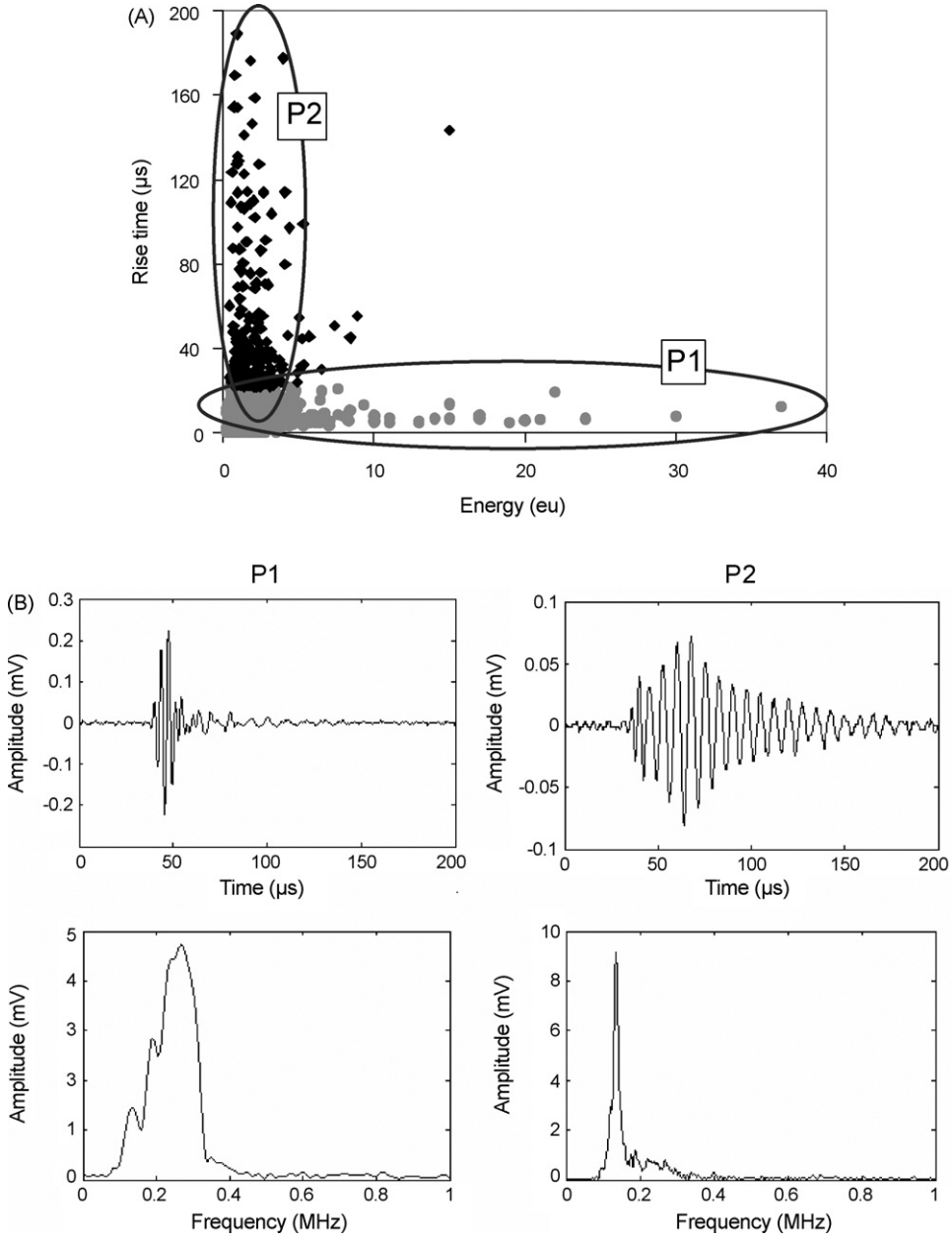

Fig. 3. (A) Rise time vs. signals energy recorded during charge at $-100\,mA\,g^{-1}$ on a $LaNi_5$-based electrode. (B) Typical waveforms and associated power spectra of recorded AE signals during charge at $-100\,mA\,g^{-1}$ on a $LaNi_5$-based electrode.

A first one, with short rise time (≈10 μs) and high amplitude (≈0.25 mV) can be correlated to P1 and shows a peak frequency between 230 and 260 kHz, while the second one exhibits longer rise time (≈50 μs) and smaller amplitude (≈0.07 mV), with a peak frequency between 150 and 180 kHz. On the basis of literature data related to the study of corrosion processes by acoustic emission [13,14], the parameters of the P2 signals are typical of acoustic signals generated from the evolution of hydrogen bubbles in contrast to the P1 signals. Furthermore, preceding AE studies on metal hydride electrodes [11,12] have shown that pulverization phenomena have a wider frequency distribution than those generated from HER, as well as higher energy, duration and rise time, which is also observed in our case for the P1 set of signals. Hence, P1 can be attributed to pulverisation phenomena whereas P2 is due to the formation of H_2 bubbles. Their respective characteristics are reported in Table 1. As confirmation, similar AE experiment was performed on a Cu electrode and then, only P2 acoustic signals related to HER were detected as seen in Fig. 4.

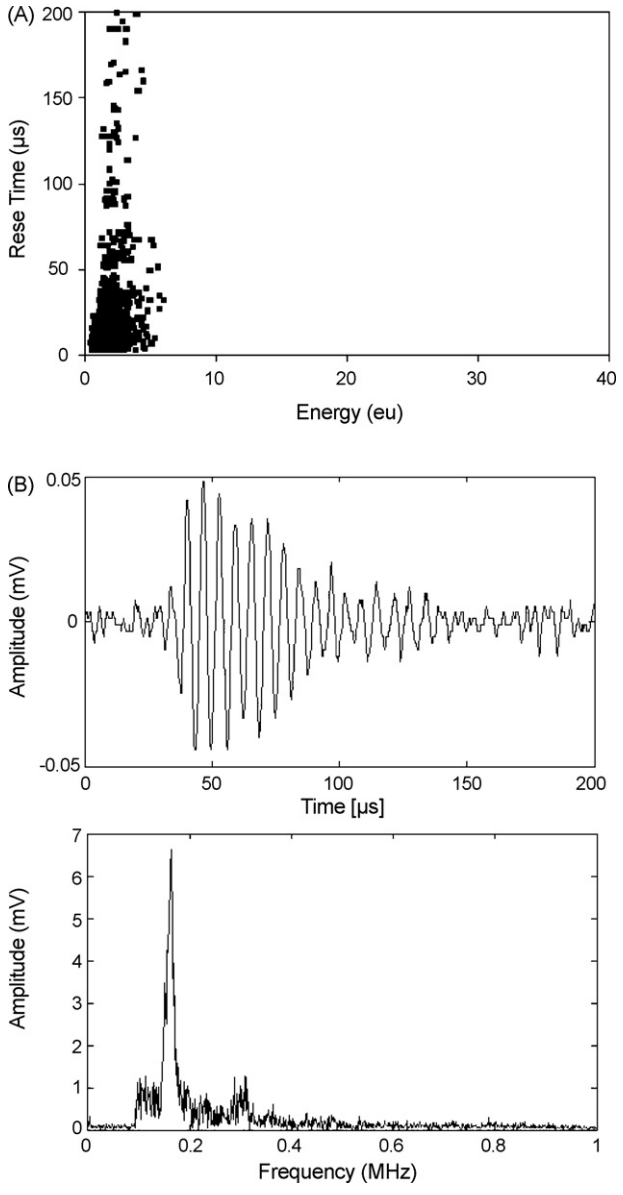

Fig. 4. (A) Rise time vs. signals energy recorded at −100 mA g^{-1} on a Cu electrode. (B) Typical waveforms and associated power spectra of recorded AE signals at −100 mA g^{-1} on a Cu electrode.

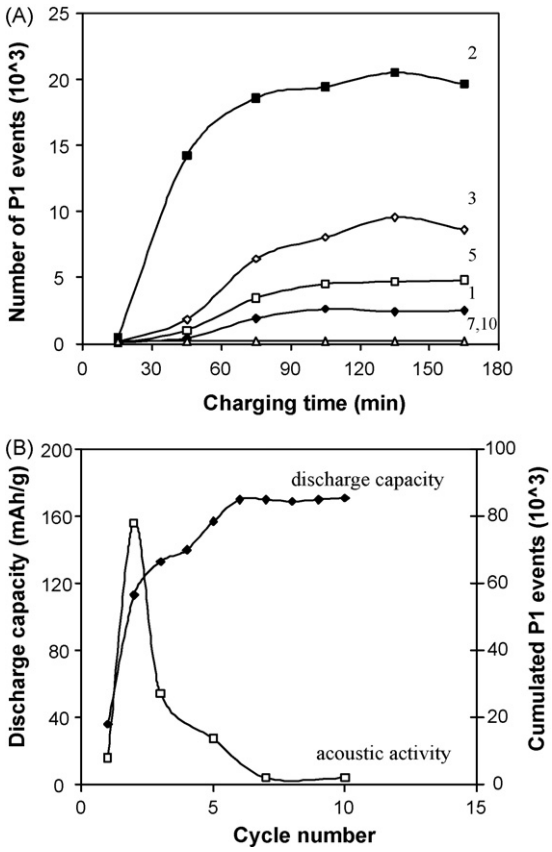

Fig. 5. (A) Evolution of population P1 during charging through cycling on the $LaNi_5$-based electrode. (B) Correlation between discharge capacity and cumulated P1 acoustic activity on the $LaNi_5$-based electrode.

3.3. Evolution of population P1 through cycling

Populations have been discriminated by their peak frequency and counted using Microsoft Excel software. The evolution of population P1 through cycling for the $LaNi_5$-based alloy (cycles 1, 2, 3, 5, 7 and 10) and the MgNi alloy (cycle 1, 2, 5, 7) is presented in Figs. 5 and 6A–B, respectively. Note that the maximum discharge capacity values indicated in Figs. 5 and 6B are ∼20–30% lower than those expected because some part of the active material in the working electrode is not electrochemically accessible probably due to the electrode compactness and the presence of the seal partially covering the sample as seen in Fig. 1.

From Fig. 5A, we can see that acoustic activity related to pulverisation phenomena on the $LaNi_5$-based electrode is low for the first cycle, reaches its maximum at the second cycle and decreases to become almost nonexistent from cycle seven. This can be correlated to the evolution of the electrode discharge capacity (Fig. 5B). Indeed, the greatest increase in discharge capacity is observed between cycles 1 and 2, whilst P1 acoustic activity is at its maximum during the second cycle. Between

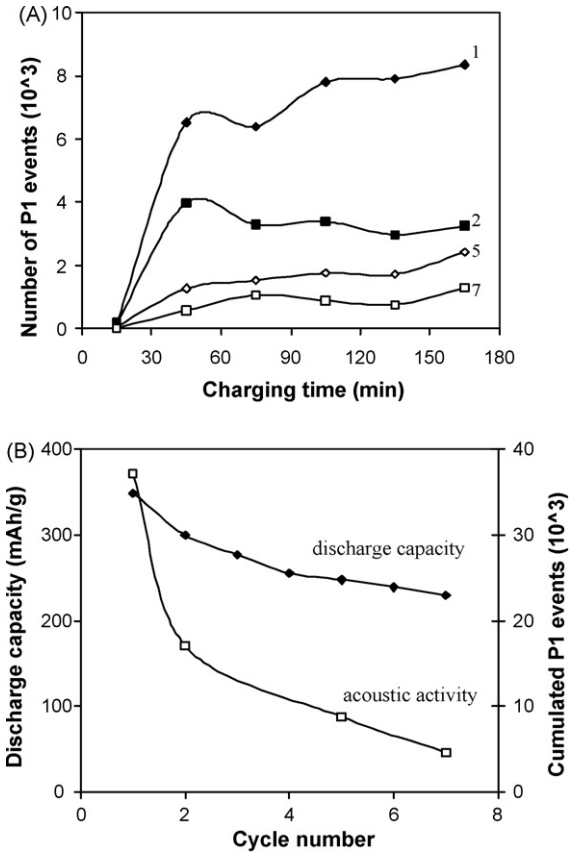

Fig. 6. (A) Evolution of population P1 during charging through cycling on the MgNi electrode. (B) Correlation between discharge capacity and cumulated P1 acoustic activity on the MgNi electrode.

cycles 2 and 3, the increase in discharge capacity is much lower, and acoustic activity related to P1 is also lower. Finally, the increase in discharge capacity between following cycles decreases continuously, as well as P1 activity. These observations confirm that the evolution of the discharge capacity is mainly due to pulverisation processes, by formation of new surfaces, and that they mostly happen in the five first cycles, with a maximum acoustic activity at the second cycle.

Concerning the MgNi alloy, pulverisation phenomena decrease throughout the cycling, with a maximum in P1 activity at the first charge (Fig. 6A). We can also correlate this acoustic activity with the evolution of the cycling discharge capacity (Fig. 6B). In contrast to what was observed on the $LaNi_5$-based alloy, the MgNi particle cracking does not activate the electrode but rather, it induces capacity decay. Actually, powder disintegration accelerates the formation of $Mg(OH)_2$, which consumes active material and limits the charge transfer reaction [15]. This different behaviour as regards to particle cracking reflects the higher sensitivity of the MgNi alloy to oxidation in comparison to $LaNi_5$-based alloys.

On the other hand, the maximum number of P1 events is larger for the $LaNi_5$-based alloy than for the MgNi alloy (80×10^3 and 38×10^3 events as seen in Figs. 5 and 6B, respectively), which seems to indicate that the pulverization phenomenon is less intensive on the MgNi electrode than on the $LaNi_5$-based electrode. As argued in a previous study [3], it would be related to the amorphous character of the MgNi alloy favoring a gradual volume expansion upon hydrogen absorption in contrast to crystalline $LaNi_5$-based compounds characterized by an abrupt α-to-β lattice expansion. In addition, it is well known that the particle size of the active material (not controlled in the present study) can influence greatly the electrode pulverization [16]. The influence of the MH particle size on the AE activity will be studied in a future work.

To conclude, our results demonstrated that AE technique coupled to electrochemical measurements can be successfully applied for the *in-situ* monitoring of the particle cracking of metal hydrides upon cycling. This method offers the ability to quantify the particle disintegration process and then, it would become a powerful tool in the evaluation/optimization of new metal hydrides for advanced Ni–MH batteries.

References

[1] P.H.L. Notten, R.E.F. Einerhand, J. Alloys Compd. 210 (1994) 221.
[2] J.J.G. Willems, Philips J. Res. 39 (1984) 1.
[3] S. Ruggeri, L. Roué, J. Power Sources 117 (2003) 260.
[4] M. Geng, J. Han, F. Feng, D.O. Northwood, J. Electrochem. Soc. 146 (1999) 2371.
[5] C. Rongeat, L. Roué, J. Electrochem. Soc. 152 (2005) A1354.
[6] American Society for the Testing of Materials, Standard definitions of terms relating to acoustic emission, STM E610-82, 1982.
[7] M. Fregonesse, H. Idrissi, H. Mazille, L. Renaud, Y. Cetre, Corros. Sci. 43 (2001) 627.
[8] B. Assouli, A. Srhiri, H. Idrissi, NDT and E Int. 36 (2003) 117.
[9] B. Assouli, F. Simescu, G. Debicki, H. Hidrissi, NDT and E Int. 38 (2005) 682.
[10] R. Ramesh, C.K. Mukhopadhyay, T. Jayakumar, B. Raj, Scripta Mater. 38 (1997) 661.
[11] H. Inoue, R. Tsuzuki, S. Nohara, C. Iwakura, Electrochem. Solid-State Lett. 9 (2006) 504.
[12] H. Inoue, R. Tsuzuki, S. Nohara, C. Iwakura, J. Alloys Compd. 446–447 (2007) 681.
[13] H. Idrissi, J. Derenne, H. Mazille, J. Acoustic Emission 18 (2000) 409–416.
[14] F. Bellenger, H. Mazille, H. Idrissi, NDT and E Int. 35 (2002) 385–392.
[15] S. Ruggeri, L. Roué, J. Huot, R. Schulz, L. Aymard, J.M. Tarascon, J. Power Sources 112 (2002) 547.
[16] C. Rongeat, L. Roué, J. Power Sources 132 (2004) 302.